JOURNAL OF GEOPHYSICAL RESEARCH, VOL. 89, NO. C4, PAGES 6467–6476, JULY 20, 1984

Estimates of the Joint Statistics of Amplitudes and Periods of Ocean Waves Using an Integral Transform Technique

K. T. SHUM AND W. K. MELVILLE

Department of Civil Engineering, R. M. Parsons Laboratory, Massachusetts Institute of Technology

An integral transform method is used to obtain continuous time series of wave amplitude and period from ocean wave measurements. The joint statistics of these two variables are determined and directly compared with the theoretical probability densities predicted by Longuet-Higgins (1975, 1983). Good agreement is found for data from both calm and hurricane sea states. This method avoids the ambiguities in the definitions of wave amplitude and period found in earlier comparisons of field data with theory.

1. INTRODUCTION

A knowledge of the joint probability density (JPD) of ocean wave heights and periods is of interest to oceanographers and engineers. Such distributions complement the power spectral estimates by providing information on the signal in the time domain rather than the frequency domain. Despite the practical importance of having good estimates of the JPD, especially for extreme wave conditions, considerable ambiguity exists in the comparisons of the available theoretical distributions with those obtained from field data. Much of this ambiguity arises from the definitions of wave height and period used in data analysis, which are usually rather arbitrary. The most popular definition is based on a "zero-crossing wave" defined as the part of record between alternate zero crossings of the water surface. The wave amplitude is then defined as the maximum displacement of the water level between zero crossings and the wave period is the interval between alternate crossings. However, available theories on the statistical distributions of these two variables involve approximations that apply only for waves from narrow band spectra.

In this paper an integral transform technique is used to uniquely define the amplitude and period as continuous functions of time for a given wave record. The main advantages of this method are that it corresponds directly to the usual theoretical descriptions, with essentially no arbitrariness, and that it lends itself to fast and efficient implementation through the use of the fast Fourier transform. A similar technique was employed by *Naess* [1982] to deduce the extrema of the wave envelope (defined as the magnitude of $\rho(t)$ in (2) below) for the case of a narrow band spectrum, by *Melville* [1983] to analyze laboratory measurements of the instabilities of deep-water waves, and by *Tayfun* [1983] to compare the envelope approach with conventional crest-to-trough distributions of wave height measurements. However, the method does not appear to have been previously used to obtain the joint density of amplitude and period of ocean waves.

The general problem of finding the JPD of ocean waves was considered by *Longuet-Higgins* [1975]. His treatment is based on the idea of Fourier analysis, i.e., the wave field $\zeta(t)$ is the sum of a large number of sinusoidal components of different frequencies and random phases,

$$\zeta(t) = \sum_{n=1}^{M} A_n \cos(\sigma_n t + \phi_n) \tag{1}$$

in which A_n is the (real) amplitude, σ_n is the angular frequency, and ϕ_n is the phase angle of the nth component. The function $\zeta(t)$ can also be written as

$$\mathrm{Re}\left\{\sum_{n=1}^{M} A_n \exp[i(\sigma_n t + \phi_n)]\right\} = \mathrm{Re}\{\rho(t)e^{i\theta(t)}e^{i\langle\sigma\rangle t}\} \tag{2}$$

in which $\rho(t)e^{i\theta(t)}$ can be expressed as

$$\sum_{n=1}^{M} A_n \exp\{i[(\sigma_n - \langle\sigma\rangle)t + \phi_n]\}$$

and is the complex envelope function of amplitude $\rho(t)$ and phase $\theta(t)$, modulating the carrier wave $e^{i\langle\sigma\rangle t}$. The mean frequency $\langle\sigma\rangle$ was chosen such that the first moment of the frequency spectrum μ_1 vanishes, where

$$\mu_r = \sum_{n=1}^{M} \frac{1}{2}(\sigma_n - \langle\sigma\rangle)^r A_n^2 \tag{3}$$

The joint density of ρ and $\dot{\theta}$ was then obtained by applying the Law of Large Numbers, assuming that the number of components, M, is large. It takes the form

$$p(\rho, \dot{\theta}) = \frac{\rho^2}{\mu_0}(2\pi\mu_2)^{-1/2} \exp\left\{-\frac{\rho^2}{2}\left[\frac{1}{\mu_0} + \frac{\dot{\theta}^2}{\mu_2}\right]\right\} \tag{4}$$

which is the fundamental result of *Longuet-Higgins* [1975]. However, not all values of ρ and

$$\tau = \frac{2\pi}{\langle\sigma\rangle + \dot{\theta}} \tag{5}$$

in this theoretical distribution correspond to values of zero-crossing amplitudes and periods. To compare this theoretical distribution with actual wave records, only those values of ρ at the wave crests should be taken into account, with the wave period being the interval between succeeding instants at which the phase function $\theta(t) + \langle\sigma\rangle t$ equals multiples of 2π. To avoid such complications, the narrow band assumption was introduced. This required that the energy spectrum of the surface wave concentrates around some mean frequency. The wave record can therefore be considered as a simple sinusoidal carrier wave with a slow amplitude modulation. The distribution of wave crests can then be approximated by that of the amplitude function ρ and that for wave period can be evaluated from a binomial expansion about the mean frequency in the expression for the joint statistics:

$$\frac{2\pi}{\dot{\theta} + \langle\sigma\rangle} \doteq \frac{2\pi}{\langle\sigma\rangle}\left(1 - \frac{\dot{\theta}}{\langle\sigma\rangle}\right)$$

This approximate density, however, failed to describe the

Paper number 4C0295.
0148-0227/84/004C-0295$05.00

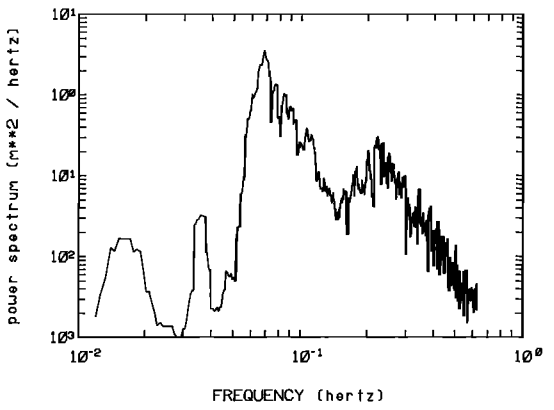

Fig. 1. Logarithmic plot of the power spectrum for the data from the Pacific Ocean over 1.75 hours sampling at 2.60 hertz. Each value is an arithmetic mean of seven adjacent frequency components centered about that frequency.

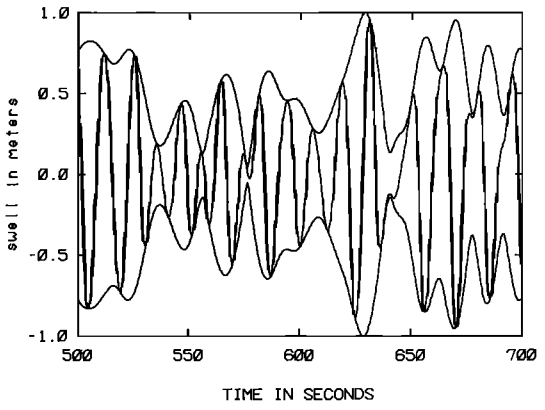

Fig. 2. A band-passed wave record and its envelope function over 200 seconds for band pass [I] (swell) of data from the Pacific Ocean; $\nu = 0.21$.

asymmetry about the mean frequency in the joint statistics as found in wave data of finite bandwidth spectra.

In the above derivation, the joint distribution of zero-crossing amplitudes and periods were obtained from an asymptotic expansion (as the bandwidth approaches zero) of the joint distribution of the continuous amplitude and phase function. This approximation led to limitations on the bandwidth for which the expressions are valid. Moreover, the zero-crossing definitions become arbitrary as the waves become irregular and have multiple extrema in between crossings. We shall therefore make a more direct comparison between theoretical densities and wave data. Instead of the zero-crossing wave, we will define the amplitude and period as time series which can be deduced from the water surface elevation record $\zeta(t)$. Assuming that $\zeta(t)$ can be formulated as in (2), the imaginary part of $\rho(t)e^{i\theta(t)}e^{i\langle\sigma\rangle t}$ is given by the Hilbert transform of the original surface elevation under the restriction that the function $\rho(t)e^{i\theta(t)}e^{i\langle\sigma\rangle t}$ has no negative frequency components in its Fourier transform domain. With both real and imaginary parts of the complex function known, time series of amplitude $\rho(t)$ and phase $\theta(t) + \langle\sigma\rangle t$ (and hence frequency) are readily obtained. The details of this procedure are given in the appendices.

TABLE 1. Parameters for the Various Band Passes Studied and the Range and Chi-Square Values for the Corresponding Histograms

	Band Pass			
	Calm Sea			
Data	[I]	[II]	[III]	Hurricane Sea
Range of band pass, s	6.9–20.0	2.4–6.9	1.5–25.0	2.0–20.0
ν	0.21	0.24	0.73	0.41
$\langle\tau\rangle$, s	12.7	4.0	7.6	10.2
μ_0, m^2	0.120	0.044	0.167	10.11
$1 - K$	0.981	0.984	0.877	0.944
L	0.981	0.983	0.876	0.942
Wave slope	0.017	0.106	0.057	0.246
	Parameters for the Histograms			
Amplitude				
Range, m	0.06–1.44	0.04–0.96	0.075–1.80	0.6–14.4
Degrees of freedom	48	45	45	24
Chi-square values	163	72	63	48
Wave period				
Range, s	1.0–29.0	1.5–13.0	2.5–37.0	3.2–30.8
Degrees of freedom	47	47		24
Chi-square values	144	38	307	102

The parameters ν, $\langle\tau\rangle$, μ, K, L, and chi-square values are given in (9), (8), (3), (C6), (C9), and (11), respectively.

The initial aim of the work reported here was to test the fundamental result of *Longuet-Higgins* [1975] ((4) above) against field data by applying this demodulation technique and avoiding the additional approximations that led to the symmetric distributions. During the course of this work it was learned that some of our results had been anticipated by *Longuet-Higgins* [1983]. In this most recent paper, it was shown that that the JPD is given by

$$p(R, T) = \left\{\frac{2}{\nu\sqrt{\pi}}\frac{R^2}{T^2}\exp\left[-R^2\left(1 + \left(\frac{1}{T} - 1\right)^2\Big/\nu^2\right)\right]\right\} L(\nu) \tag{6}$$

where

$$R = \rho/(2\mu_0)^{1/2} \tag{7a}$$

$$T = \tau/\langle\tau\rangle \tag{7b}$$

are the nondimensional amplitude and period, respectively.

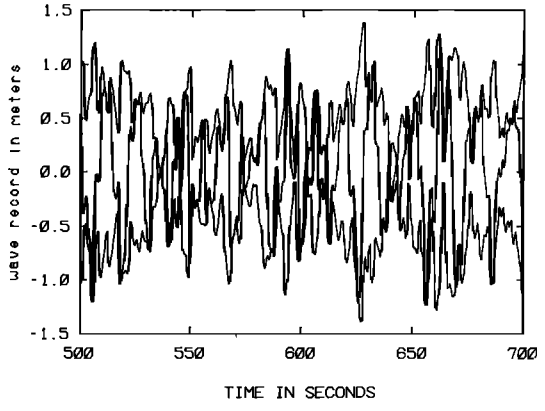

Fig. 3. A wave record and its envelope function over 200 seconds for band pass [III] of data from the Pacific Ocean, $\nu = 0.73$.

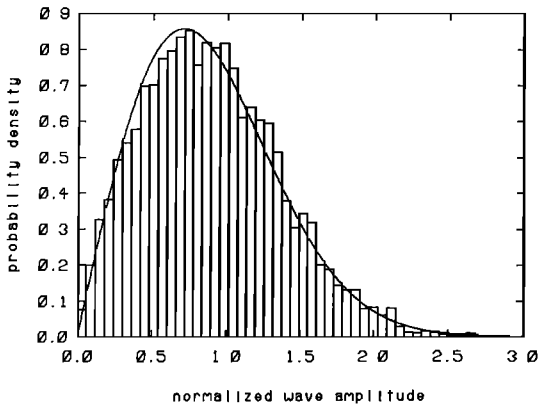

Fig. 4. Histogram of wave amplitude for band pass [I] (swell) of the Pacific Ocean data over 1.40 hours sampling at 2.60 hertz. The curve is the Rayleigh distribution. Density values are per unit normalized amplitude; $(2\mu_0)^{1/2} = 0.490$ m.

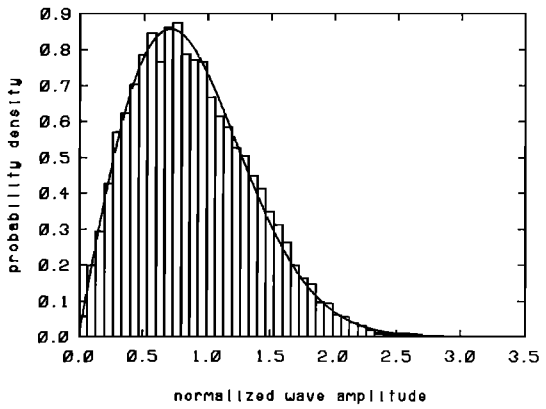

Fig. 6. Histogram of wave amplitude for band pass [III] of the Pacific Ocean data over 1.4 hours sampling at 2.60 hertz. The curve is the Rayleigh distribution. Density values are per unit normalized wave amplitude; $(2\mu_0)^{1/2} = 0.578$ m.

The rth moment μ_r is defined as in (3), and

$$\langle\sigma\rangle = 2\pi/\langle\tau\rangle \tag{8}$$

is chosen such that $\mu_1 = 0$. The function

$$L(\nu) = \tfrac{1}{2}[1 + (1 + \nu^2)^{1/2}] \approx 1 + \nu^2/4 + 0(\nu^2)$$

is a normalization factor to account for the probability of negative frequencies in (4) which should not exist. The dimensionless parameter ν, which increases with bandwidth, is given by

$$\nu = \frac{1}{\langle\sigma\rangle}(\mu_2/\mu_0)^{1/2} \tag{9}$$

The aim of this paper, then, is to compare directly the above thoeretical distribution with the statistics of the amplitude and period as evaluated by the Hilbert transform. Field data obtained in the Pacific Ocean and the Gulf of Mexico are used for comparisons of the measured statistics with theoretical joint distributions.

The field data and methods of analysis are described in section 2. The results are presented in section 3 and discussed in section 4. A brief review of Hilbert transform technique and the theoretical joint density of wave amplitude and period proposed by *Longuet-Higgins* [1983] are given in Appendices A and B. The form of the distribution appropriate in the analysis of digital data is introduced in Appendix C.

2. Field Data and Analysis

Two sets of data were analyzed, one from a mild sea state and the other from hurricane conditions. The unpublished field data from a relatively calm sea were made available by R. E. Davis and L. Regier of the Scripps Institution of Oceanography, La Jolla, California. Measurements were made from the Floating Instrument Platform (FLIP) which was stationed at 31.52°N, 118.30°W in the Pacific Ocean, 250 miles west of San Diego, California in water between 3000 m and 4000 m deep. The data were taken on March 26, 1973 starting at 1700 Pacific Standard Time under calm weather. The record included measurements from resistance wave gages and the pitch and roll motions of FLIP. Individual channels were digitized simultaneously (within 50 μs of each other) at a frequency of 2.60 cycles per second from recorded analog data. A total of 2^{14} (= 16,384) data points spanning 6291 seconds (1.75 hours) were used, giving a time interval between data points of 0.384 s, a frequency resolution of 1.59×10^{-4} s^{-1}, and a Nyquist frequency of 1.30 s^{-1} in the digital Fourier transform.

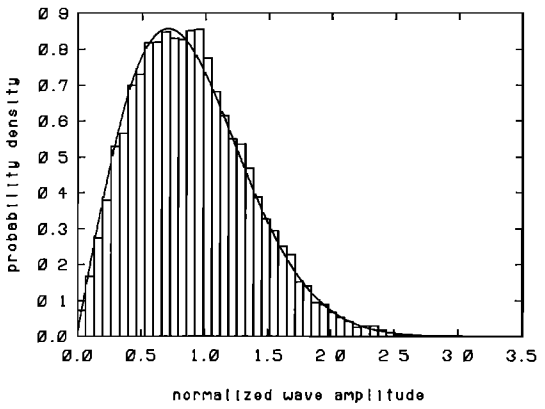

Fig. 5. Histogram of wave amplitude for band pass [II] (wind wave) of the Pacific Ocean data over 1.40 hours sampling at 2.60 hertz. The curve is the Rayleigh distribution. Density values are per unit normalized wave amplitude; $(2\mu_0)^{1/2} = 0.297$ m.

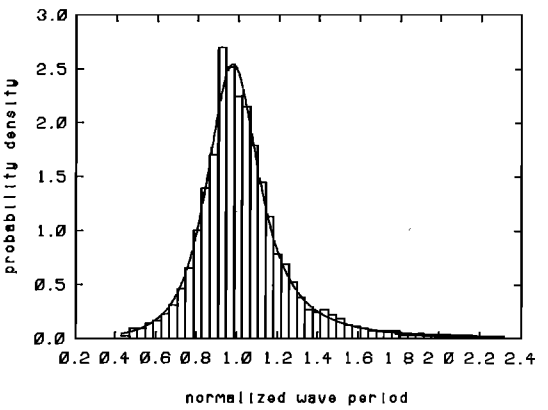

Fig. 7. Histogram of 12914 values of wave period for band pass [I] (swell) of the Pacific Ocean data. The curve is the theoretical distribution as given by (C4) and (C5). Density values are per unit normalized period; $\langle\tau\rangle = 12.7$ s, $\nu = 0.21$.

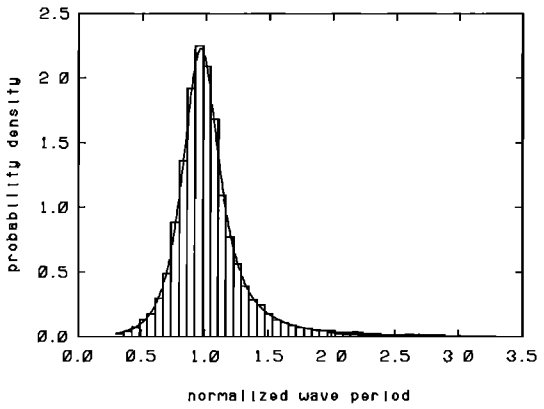

Fig. 8. Histogram of 12898 values of wave period for band pass [II] (wind wave) of the Pacific Ocean data. The curve is the theoretical distribution as given by (C4) and (C5). Density values are per unit normalized period, $\langle\tau\rangle = 4.0$ s, $\nu = 0.24$.

The wave gage measurement was corrected for the pitch and roll of FLIP. Since the magnitude of these two angles rarely exceeded a few degrees, the change in elevation due to pitch and roll motion can be approximated by the product of this angle and the distance between the gage and the center of hull projected along the corresponding axis of rotation. The adjusted gage reading was then found by subtracting this product from the original record. The contribution from the vertical and lateral translations of FLIP were not accounted for since these quantities were not readily measurable. The natural frequency for heave motion of FLIP was approximately 0.037 Hz (27 s), while that for pitch and roll motion was near 0.021 Hz (48 s). These frequencies were prominent in the energy spectra but below the frequency range of the wave field. They were filtered out by high passing the time series above 0.04 Hz.

The second set of data was recorded in the Ocean Data Gathering Program (ODGP) in the Gulf of Mexico and furnished to us by G. Z. Forristall of Shell Development Company. It was taken by an inductance wave staff mounted within the legs of an oil rig in 340 feet (~ 100 m) of water (ODGP station 1). Further details of the measurements can be found in papers by *Hamilton and Ward* [1974], *Ward* [1974], and *Patterson* [1974]. The record in this analysis was taken on August 17, 1969. The data started at 1500 CST when the

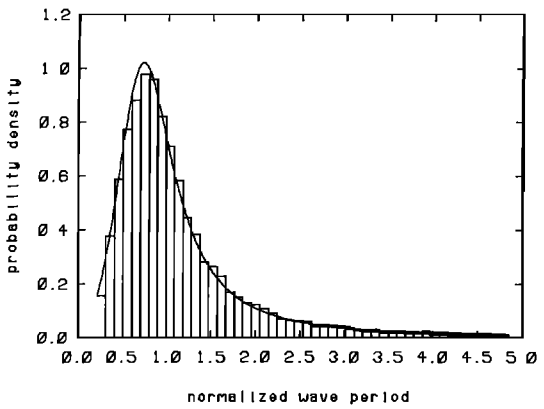

Fig. 9. Histogram of 11245 values of wave period for band pass [III] of the Pacific Ocean data. The curve is the theoretical distribution as given by (C4) and (C5). Density values are per unit normalized period; $\langle\tau\rangle = 7.6$ s, $\nu = 0.73$.

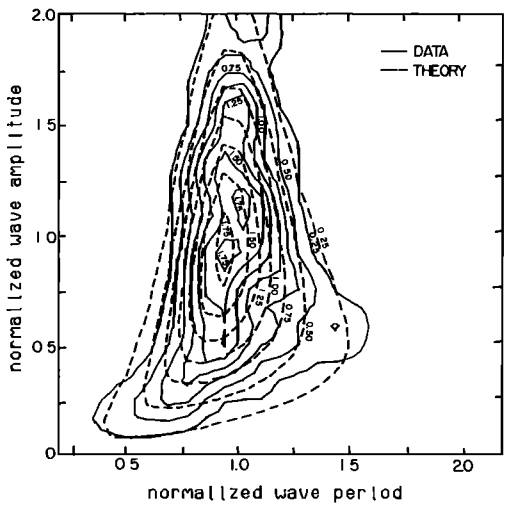

Fig. 10. Joint distribution of 12914 pair of values of amplitude and period at 2.60 hertz for band pass [I] (swell) of the Pacific Ocean data. Density values are per unit normalized amplitude per unit normalized period; $\nu = 0.21$, $(2\mu_0)^{1/2} = 0.490$ m, $\langle\tau\rangle = 12.7$ s.

eye of hurricane Camille was within 30 miles (48 km) of the structure. It lasted for 4096 seconds, with data points uniformly spaced at 1-second intervals, giving a frequency resolution of 2.4×10^{-4} s^{-1} and a Nyquist frequency of 0.5 s^{-1} in the digital Fourier transform. The significant wave height increased from 39.5 ft (12.0 m) to 43.0 ft (13.1 m) over this time span [*Patterson*, 1974].

Each wave record was filtered with a tapered cosine window of length one tenth its duration. This reduced the leakage of the spectrum [see *Bingham et al.*, 1967] and decreased the total energy in the spectrum by 12.5%. To account for this reduction in energy, the averages of one half sum of squares of the records at each stage in the analysis above were calculated for comparison. In particular, the ratio of the sum of squares of the records before and after the cosine window was found. The square root of this ratio was multiplied to the digital Fourier transform coefficients of the filtered function to compensate for this loss of energy in the cosine window.

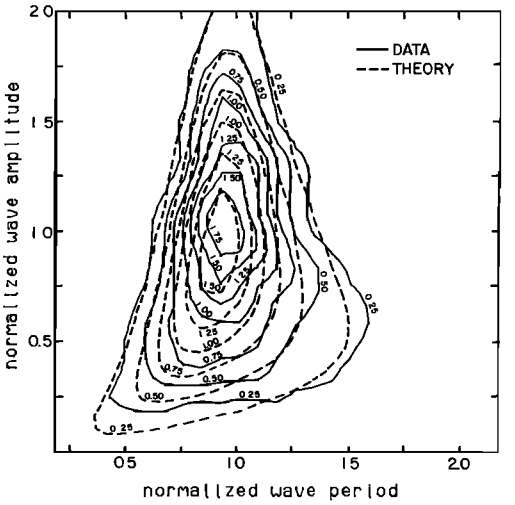

Fig. 11. Joint distribution of 12898 pair of values of amplitude and period at 2.60 hertz for band pass [II] (wind wave) of the Pacific Ocean data. Density values are per unit normalized amplitude per unit normalized period; $\nu = 0.24$, $(2\mu_0)^{1/2} = 0.297$ m, $\langle\tau\rangle = 4.0$ s.

A band pass was then applied to the spectrum. The moments μ_r for each bandpass were evaluated. The Hilbert transform was taken, and the wave amplitude and period derived as discussed in the appendices. Histograms for these two parameters were then plotted using only those data points inside the tapered ends of the cosine window. The range of wave period was, however, limited to the fundamental range, as discussed in Appendix C, and all wave periods outside this range were discarded. Their joint densities are presented as contour maps in which, as in the histogram for wave periods, only data points with periods inside the fundamental range ($2/f$, 50 s) were used (f is the sampling frequency in samples per second). This restriction on the range of wave period required a modified expression for the theoretical densities, as derived in Appendix C. A smoothing technique was employed in the contouring in which the modified joint density value at each grid point was a weighted average of its original value and its eight neighboring points, i.e.,

$$\begin{aligned} x^*(i,j) = x(i,j)/4 &+ [x(i-1,j) + x(i+1,j) \\ &+ x(i,j-1) + x(i,j+1)]/8 \\ &+ [x(i-1,j-1) + x(i+1,j-1) \\ &+ x(i+1,j+1) + x(i-1,j+1)]/16 \end{aligned}$$

in which $x(i, j)$ was the original density value at grid point (i, j) and $x^*(i, j)$ was the smoothed value. This smoothing technique was applied to both field data and theoretical curves. The subroutine for this contouring determined the location of the contours by linear interpolation of the density values at adjacent grid points.

3. Results

3.1. *Calm Sea (Pacific Ocean)*

The power spectrum (Figure 1) consists of two dominant peaks: one of period between 8 and 18 s, the other between 3 and 6 s. The peaks at periods greater than 25 seconds are believed to be due to the pitch and roll motions of FLIP and are therefore filtered out. Three band passes were thus chosen in our study. The first [I] from 6.9 s to 20 s corresponds to the swell and accounts for 69% of the total energy. The second band pass [II] from 2.36 s to 6.9 s corresponding to the wind waves accounts for 26% of the total energy. The third [III] between 1.5 s and 25 s includes both wind waves and swell and contains over 98% of the total energy. Various parameters for these band passes are presented in Table 1, wherein "wave period" refers to the range in frequency domain of the band pass. The parameters ν, $\langle\tau\rangle$, μ_0, K, and L in Table 1 are given by (9), (8), (3), (C6), and (C9), respectively. The characteristic wave slope is defined as

$$\langle k\rangle 2\sqrt{\mu_0} \tag{10}$$

in which $\langle k\rangle$ is the wave number corresponding to $\langle\tau\rangle$, using linear one-dimensional wave theory, and $2\sqrt{\mu_0}$ is a measure of the wave amplitude.

Figure 2 shows a sample record over 200 seconds of band pass [I]. The upper and lower curves are the envelope function as obtained from the Hilbert transform (C1). It is interesting to note that most maxima of the actual record coincide with that of the envelope. However, if we define the interval between adjacent maxima (or minima) as a period, it is seen that the periods for the envelope are only about three to four times that of the actual record. Thus the basic assumption mady by *Longuet-Higgins* [1975], that the extrema of the sur-

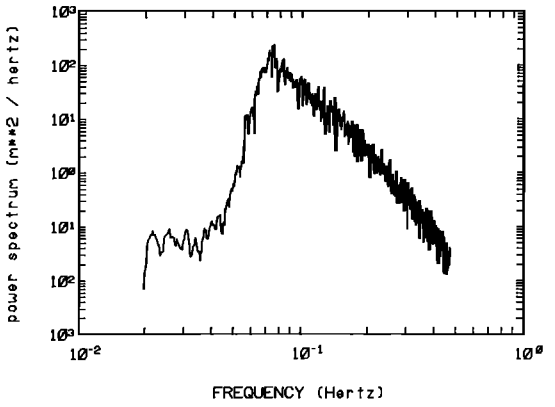

Fig. 13. Power spectrum of hurricane Camille over 4096 seconds sampled at 1 hertz. Each value is an arithmetic mean of seven adjacent frequency components centered about the frequency.

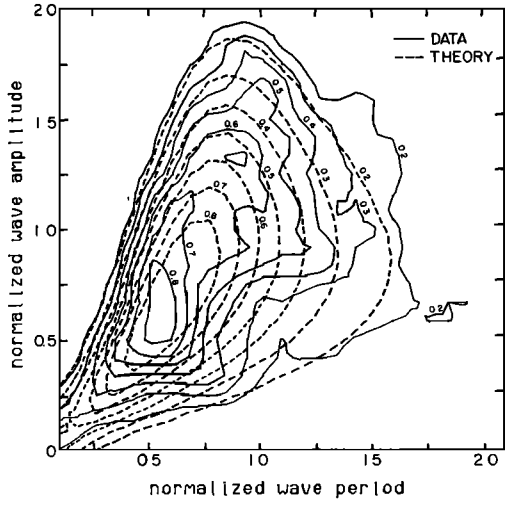

Fig. 12. Joint distribution of 11245 pair of values of amplitude and period at 2.60 hertz for band pass [III] of the Pacific Ocean data. Density values are per unit normalized amplitude per unit normalized period; $\nu = 0.73$, $(2\mu_0)^{1/2} = 0.578$ m, $\langle\tau\rangle = 7.6$ s.

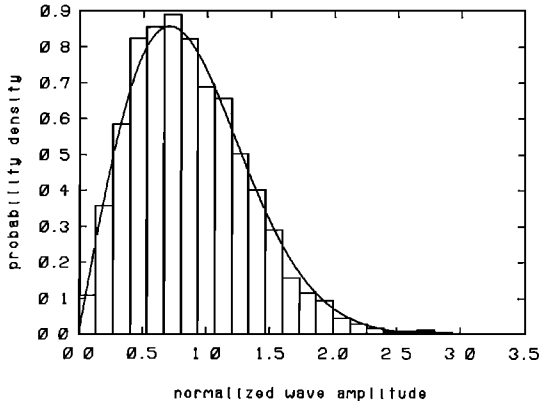

Fig. 14. Histogram of 3276 values of normalized wave amplitude for hurricane Camille sampled at 1 hertz. The curve is the Rayleigh distribution. Density values are per unit normalized amplitude; $(2\mu_0)^{1/2} = 4.50$ m.

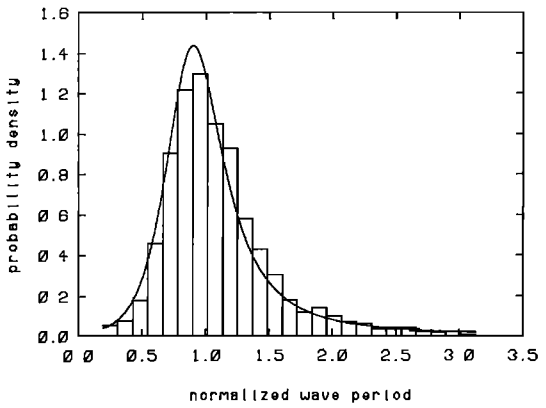

Fig. 15. Histogram of 3109 values of wave period for hurricane Camille. The curve is the theoretical distribution as given by (C4) and (C5). Density values are per unit normalized period; $\langle\tau\rangle = 10.2$ s, $\nu = 0.41$.

face elevation densely register the envelope, is not realized in this case, even though the bandwidth parameter ν^2 is considerably below the 0.36 narrow band criterion, as suggested by *Longuet-Higgins* [1983]. Figure 3 is a sample of the record and its envelope for band pass [III]. Note that the maxima of the envelope function are not always attained by the original record.

Figures 4 through 6 are histograms of the amplitude functions as derived in Appendix C (equation (C1)) for band passes [I], [II], and [III]. The solid curves are theoretical densities, as given by (B2). The probability densities are shown per unit normalized wave amplitude. The wave amplitude for the peak density values in the theory are about 0.1 unit lower than that of the statistics for band passes [I] and [II]; however, the maximum theoretical density values in all three cases agree well with those from data, particularly for the high wave amplitudes which are of most practical concern.

Figures 7 through 9 are histograms for wave period for the same band passes [I], [II], and [III] as evaluated according to (C2) and (C3). The solid curves are theoretical distributions as given by (C4). We see good agreement between the statistical properties of field data and theoretical distributions.

Figure 10 is the joint histogram and theoretical joint density (equation (C7)) for band pass [I]. Similarly, Figure 11 is for band pass [II] and Figure 12 is for band pass [III]. (The failure of the JPD contours to converge to the origin in Figures 12 and 16 is a result of the smoothing described above.) The contours are interpolated from a square grid of 25 × 25 density values. It was found that a further increase in the number of divisions led to very irregular contours in the statistics. Many of the qualitative features of the theory are seen in the data for the joint densities, as discussed by *Longuet-Higgins* [1983]; in particular, we note the increasing asymmetry in the joint distribution as bandwidth increases.

3.2. *Hurricane Sea (Camille in the Gulf of Mexico)*

The power spectrum is shown in Figure 13. It is single peaked, as is typical of storm spectra. The high-frequency components decay as the negative fifth power of frequency, which is characteristic for Pierson-Moskowitz or JONSWAP (Joint North Sea Wave Project) spectra. A bandpass of 2 s to 20 s is applied to the record and accounts for 99% of the original energy.

The histograms for amplitude and period are presented in Figures 14 and 15, respectively. The agreement is good except at the peak density values in which the values predicted by theory are lower/higher than the statistics for amplitude/period. The joint distributions are shown in Figure 16, where the contour values are per unit normalized amplitude per unit normalized period. A density value of 0.05 corresponds to 1 count of data per grid, which is the lower limit of resolution. Even though it is of interest to study the densities at high wave amplitudes, the limited sample size restrict the range of resolution of both amplitudes and periods in the joint distribution.

Chi-square tests have been performed on both sets of data to examine the goodness of fit. The chi-square values are presented at the end of Table 1. These numbers are evaluated as

$$\chi^2(I) = J \sum_{i=1}^{I+1} \frac{(f_i - n_i/J)^2}{f_i} \tag{11}$$

in which $\chi^2(I)$ is the χ^2 value with degree of freedom I, f_i is the cumulative probability in the interval i, n_i is the number of samples that have values in the same interval, $I + 1$ is the number of intervals, and J is the total number of data points. Despite the apparent good agreement found between the histograms and theoretical curves, the chi-square values have significance values of over 0.99 except for wave period in the case of wind waves (band pass [II] for the Pacific Ocean data). (I.e., if the theoretical curves were to agree with the experimental measurements, there would be less than a 1% chance that the chi-square values are as large as shown here.)

4. Discussion

It has been shown that the Hilbert transform technique can be applied to wave records and the amplitudes and periods thus obtained have statistical distributions in good agreement with those proposed by *Longuet-Higgins* [1983] for a bandwidth parameter ν of up to 0.73. From the mathematical point of view, there is no restrictions on the spectral bandwidth for which the derivation of the theoretical densities are valid. In other words, no limitations are placed on the frequencies of

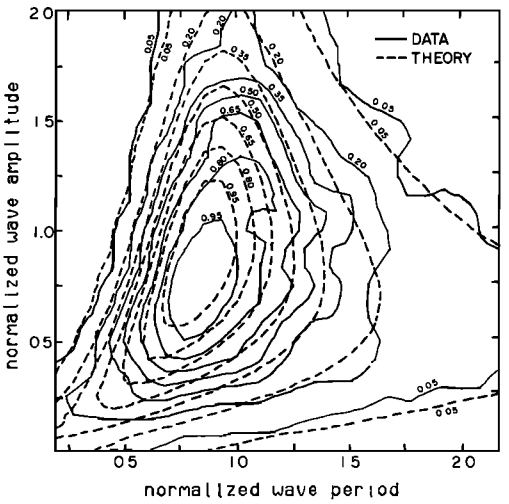

Fig. 16. Joint distribution of 3109 pairs of values for wave amplitude and period for hurricane Camille. Density values are per unit normalized period per unit normalized amplitude; $\nu = 0.41$, $(2\mu_0)^{1/2} = 4.50$ m, $\langle\tau\rangle = 10.2$ s.

the sinusoidal components in the frequency space. However, for the central limit theorem to be valid, the amplitudes of these components have to be of comparable magnitudes.

One limitation of this approach is the resolution of wave period in the time domain (as evaluated from (C2) and (C3)), being bound by the range of phase change $[\phi(t + \Delta t) - \phi(t)]$ allowed in (C3). Its upper bound depends on the value of δ (the lower limit for phase change in unit time increment; see Appendix C) and can be chosen to be arbitrarily large as long as it is short compared with the duration of the record analyzed. The lower bound is a function of the time interval between samples. This value is given by $2\Delta t$ by restricting the range of permissible phase change to (δ, π). Alternatively, we could have decreased this lower bound to Δt by defining the range of phase change to $(\delta, 2\pi)$. However, this would give a resolution of wave period below the corresponding Nyquist frequency $(= 1/2\Delta t)$ which is the limit on frequency resolution in the frequency domain. Furthermore, phase changes in the range $(\pi, 2\pi)$ can as well be interpreted as values in the range $(-\pi, 0)$ corresponding to negative frequencies [e.g., *Melville*, 1983]. To avoid this ambiguity, we limited the range of phase changes to (δ, π).

Note that the derivation of the theoretical densities requires that the wave field can be formulated as in (1) by assuming random phases ϕ_n. This necessarily requires the waves to be linear. It is shown, from the storm data, that the same theory can also be applied to sea states in which linear wave theory is no longer strictly valid. (A crude measure of the nonlinearity is given by the characteristic wave slope as defined by (10) and presented in Table 1.) It should be noted that estimating the wavelengths from the wave periods and the dispersion relationship gives an upper bound of the wave length in a wave field with an angular spread of wave incidence. (It can be easily shown, for the simple case of a two-wave system with same frequencies but different angles of incidence, that the apparent wave number calculated from records at three adjacent gages decreases from their actual value to zero as the angle included between the waves increases from 0 to π (see, for example, *Shum* [1984]).) A study of the wavenumber distribution was performed on the Pacific Ocean data using records from three wave gages. It was found that the angular spread increased with bandwidth. The estimation of nonlinearity using (10) should therefore be limited to narrow band spectra.

The hurricane wave record is from that of a growing sea as Camille approached. This time-varying excitation departs from the basic assumption of stationarity in spectral analysis, and the duration we chose (1.14 hours) is a compromise between requirements of stationarity and statistical significance.

TABLE 2. A Direct Comparison of the Goodness of Fit Between the Theoretical Distributions and Wave Data for the Various Band Passes Studied

Data	[I]	[II]	[III]	Camille
	Parameters for the Band Passes			
ν	0.21	0.24	0.73	0.41
Wave slope	0.017	0.106	0.057	0.246
	Chi-Square Values			
For amplitude	130	59	47	48
For period	94	42	92	102

Chi-square values with 24 degrees of freedom and $\approx$3200 data points.

Compared with statistical analysis of wave periods using zero-crossing waves, our present method gives a larger density value for low-frequency waves. The reason is that each wave is counted as one entry in the zero-crossing wave period statistics, while in our present method all data points are spaced equally apart in time and therefore long-period waves have more entries. This consideration applies to wave amplitude statistics as well, since large waves are associated more with low-frequency waves. However, the correspondence between the two methods in wave amplitude statistics are not as straightforward as in the case of wave periods.

From Figure 3 it is found that the maxima of the wave envelope and underlying wave record do not always coincide. This phenomenon becomes more pronounced as the spectral bandwidth increases, and some of the larger values of the envelope may not be realized by the actual waves. The statistics of this envelope function may overpredict zero-crossing amplitudes in the high values, as is observed in previous field studies [e.g., *Forristall*, 1978].

The high significance levels found in the chi-square tests suggest that the proposed theoretical models should be rejected as the distribution of the data. It is found that a significant contribution to these high χ^2 values come from only a few intervals which have large discrepancies between theory and statistics (e.g., about $T = 0.9$ in Figure 7 and $T = 0.7$ in Figure 9). Direct comparison of χ^2 values for the four wave bands studied using the same number of data points ($\sim$3200) and degrees of freedom (24) are shown in Table 2, from which it can be seen that the χ^2 values are not simply related to bandwidth or nonlinearity. From the graphs of amplitude distributions (Figures 4, 5, 6, and 14), it is seen that the location in the sample space (i.e., the nondimensional amplitudes) of the major discrepancies varies. Since the theoretical distribution (B2) does not depend on any parameters, there are no apparent remedies to correct for these high χ^2 values. We are unable to explain the failure in this χ^2 test despite the apparent good agreement observed in the graphs.

APPENDIX A: REVIEW OF HILBERT TRANSFORM

The Hilbert transform technique has been used previously in the study of amplitude and frequency modulation in water waves, for example, by *Naess* [1982] and *Melville* [1983]. A review of this transform is given below.

Let $S(t)$ be a complex signal with $\zeta(t)$ and $\eta(t)$ its real and imaginary parts. Given only the real part $\zeta(t)$ of the time history of $S(t)$, $\eta(t)$ is, in general, undetermined. However, for the special case in which the Fourier Transform of $S(t)$ has no negative frequency components, $\eta(t)$ (and thus $S(t)$) can be found from $\zeta(t)$ by the Hilbert transform technique. It was first proposed by *Dugundji* [1958]. A detailed account of this transform as applied to digital time series can be found in the work of *Oppenheim and Schafer* [1975].

Let the wave record $\zeta(t)$ be the real part of the complex signal $S(t)$ having Fourier coefficients c_n^e such that

$$\zeta(t) = \sum_{n=1}^{N-1} c_n^e e^{in\sigma t}$$

The Fourier coefficients c_n of $S(t)$ are then given by

$$c_n = 0 \qquad N/2 \le n \le N - 1$$

$$c_n = 2c_n^e \qquad 1 \le n \le N/2 - 1$$

In the time domain, $S(t)$ can be represented as $\zeta(t) + i\mathcal{H}[\zeta(t)]$

where

$$\mathcal{H}[\zeta(t)] = -\frac{1}{\pi}\int_{-\infty}^{+\infty} d\tau \frac{\zeta(\tau)}{t-\tau} = \eta(t)$$

which is the well-known Hilbert transform of σ(t).

It should be noted that this approach will give an accurate description of $S(t)$ only if it contains no negative frequency components, i.e., $c_n = 0$ for $N/2 \le n \le N-1$. This is the causality requirement in time series analysis, i.e., information does not propagate backwards in time. In other words, what happens in a subsequent moment would not change the signal at any previous instants. We shall discuss this assumption in Appendix B.

Appendix B: Relationship Between Parameters in the Joint Density of Longuet-Higgins [1983] and the Fast Fourier Transform Coefficients of the Wave Record

The wave field $\zeta(t)$ is assumed to be composed of a large number of sinusoidal components of different frequencies and random phases, as in (1). By expressing $\zeta(t)$ as the real part of $\rho(t)e^{i\theta(t)}e^{i\langle\sigma\rangle t}$ (and recall (5)), *Longuet-Higgins* [1983] was able to show that the joint distribution of wave amplitude and period in terms of nondimensional amplitude R and nondimensional period T is given by (6). In our present interpretation, negative phase increments are acceptable, and the empirical parameter $L(\nu)$ is not needed. The joint density therefore takes the form

$$p(R, T) = \frac{2}{\nu\sqrt{\pi}}\frac{R^2}{T^2}\exp\left\{-R^2\left[1+\left(\frac{1}{T}-1\right)^2\Big/\nu^2\right]\right\} \tag{B1}$$

from which,

$$p(R) = \int_{-\infty}^{+\infty} dT\, p(R, T) = 2Re^{-R^2} \tag{B2}$$

$$p(T) = \int_0^{\infty} dR\, p(R, T) = \tfrac{1}{2}\nu^2|T|[(1+\nu^2)T^2 - 2T + 1]^{-3/2} \tag{B3}$$

To apply this to our case, we note that $\zeta(t)$ can be rewritten as

$$\begin{aligned}\text{Re}\{S(t)\} &= \sum_{n=1}^{(N/2)-1} 2\,\text{Re}\{c_n{}^e e^{in\sigma t}\} \\ &= \sum_{n=1}^{(N/2)-1} 2|c_n{}^e|\cos(n\sigma t + \psi_n)\end{aligned} \tag{B4}$$

in which ψ_n is the phase of $c_n{}^e$. A comparison of (1) and (B4) shows that if we let $A_n = 2|c_n{}^e|$, $\sigma_n = n\sigma$, $\phi_n = \psi_n$, and $M = (N/2) - 1$, we can calculate the moments μ_r from $\zeta(t)$ and the densities (equations (B1), (B2), and (B3)) are then fully determined.

In the above formulation, it is apparent that if $M > (N/2) - 1$, the original assumption in the Hilbert transform (that $c_n = 0$ for $N/2 \le n \le N-1$) is violated. However, it is well known in the theory of digital Fourier transform that if the original time signal contains frequency components above the Nyquist frequency (which equals $1/2\Delta t$), their contributions will be aliased in the Fourier transform space as lower-frequency components. In the energy spectrum of the wave record we studied, the high-frequency components become negligible at a frequency much lower than the Nyquist frequency. We therefore have confidence that the above assumption is valid in our case.

Appendix C: Resolution of Wave Period

From Appendices A and B, we see that the amplitude and period at any instant can be found as follows: Assuming that $S(t) = \rho(t)e^{i\theta(t)}e^{i\langle\sigma\rangle t} = \zeta(t) + i\eta(t)$, we have

$$\rho(t) = [\zeta^2(t) + \eta^2(t)]^{1/2} \tag{C1}$$

$$\phi(t) = \theta(t) + \langle\sigma\rangle t = \arctan[\eta(t)/\zeta(t)] \tag{C2}$$

$\rho(t)$ is therefore the amplitude at time t, and the instantaneous period is evaluated as

$$\tau(t) = \frac{2\pi\Delta t}{\phi(t+\Delta t) - \phi(t)} \tag{C3}$$

Note that the wave period thus deduced is bound by two factors. In evaluating the phase function $\theta(t) + \langle\sigma\rangle t$, the principle argument (between 0 and 2π) is assumed in taking the arctangent of $\eta(t)/\zeta(t)$. The phase change between two consecutive instants is therefore in the range of $(-2\pi, 2\pi)$ plus an unknown multiple of 2π. We restrict the phase change to the range (δ, π). From (C3) above the wave period of resolution is thus bound below by $2/f$ where $1/f$ ($= \Delta t$) is the sampling interval ($f/2$ is the Nyquist frequency). The upper bound is determined by the lower cutoff value for the phase change, δ, and the maximum wave period is then given by $2\pi/(f\delta)$. In our study, δ is chosen such that the upper bound of wave period resolution is 50 s.

The results of *Longuet-Higgins* [1983] were derived using the central limit theorem. This leads to finite probability values for all values of T in $(-\infty, \infty)$ in the theoretical distributions for both wave period and joint amplitude and period. To apply these densities to our case, we have to allow for the probabilities of periods outside the primary range (T_1, T_2) where $T_1 = 2/f$ and $T_2 = 2\pi/(f\delta)$. This includes accounting for the aliasing of phase changes in intervals $(2n\pi + \delta, 2n\pi + \pi)$, $n = \cdots, -2, -1, 1, 2, \cdots$ into (δ, π) and the phase changes in the range $(2n\pi + \pi, 2n\pi + 2\pi + \delta)$ that have been neglected. We can therefore formulate the modified density $p^*(T)$ as

$$\begin{aligned} p^*(T) &= \alpha q(T) \qquad 2/f < T < 50 \\ p^*(T) &= 0 \qquad \text{otherwise.}\end{aligned} \tag{C4}$$

where $q(T)$ is the sum of the original probability density at T and that due to aliasing and α accounts for the "lost" probability due to the exclusion of phase changes in the intervals $(2n\pi + \pi, 2n\pi + 2\pi + \delta)$, $n = \pm 1, \pm 2, \pm 3, \cdots$

It can be shown that

$$q(T) = \sum_{n=-\infty}^{\infty} J_n p(T_n) \tag{C5}$$

where

$$T_n = \frac{T}{1 + nT\langle\tau\rangle f}$$

and J_n is the Jacobian

$$\frac{\partial T_n}{\partial T} = \frac{1}{(1 + nT\langle\tau\rangle f)^2}$$

The parameter α equals $1/(1-K)$ where K is the integral of

$p(T)$ over the ranges

$$\left(-\infty, \frac{-2}{f\langle\tau\rangle}\right) \quad \left(-\frac{1}{m-\beta}\frac{1}{f\langle\tau\rangle}, -\frac{1}{m+0.5}\frac{1}{f\langle\tau\rangle}\right)$$
$$\left(\frac{1}{m+\beta}\frac{1}{f\langle\tau\rangle}, \frac{1}{m-0.5}\frac{1}{f\langle\tau\rangle}\right) \quad \left(\frac{1}{\beta}\frac{1}{f\langle\tau\rangle}, \infty\right)$$

where $m = 1, 2, 3, \cdots$ and $\beta = \delta/2\pi$. From Appendix D, we can express

$$K = \sum_{m=1}^{\infty}\left[P\left(-\frac{1}{m+0.5}\frac{1}{f\langle\tau\rangle}\right) - P\left(-\frac{1}{m-\beta}\frac{1}{f\langle\tau\rangle}\right) + P\left(\frac{1}{m-0.5}\frac{1}{f\langle\tau\rangle}\right) - P\left(\frac{1}{m+\beta}\frac{1}{f\langle\tau\rangle}\right)\right] + P\left(\frac{-2}{f\langle\tau\rangle}\right) - P\left(\frac{1}{\beta}\frac{1}{f\langle\tau\rangle}\right) \tag{C6}$$

in which $P(T)$ is given by (D4). In actual computation the infinite sum is truncated when the next term in the sum does not change by more than 10^{-5} of the previous sum. It was found that this takes no more than two terms.

For the joint density, $p(T_n)$ in (C5) should be replaced by $p(R, T_n)$, and K is the integral of $p(R, T)$ over the same ranges of T divided by $2R \exp(-R^2)$. To obtain the theoretical values for the distribution in $(R_1, R_2; T_1, T_2)$, we note that the sum of probability in this range plus the aliasing contributions is given by

$$\frac{1}{1-\kappa}\left\{Q(R_1, R_2; T_1, T_2) + \sum_{\substack{n=-\infty \\ n\neq 0}}^{\infty} Q\left(R_1, R_2; \frac{T_1}{1+nT_1\langle\tau\rangle f}, \frac{T_2}{1+nT_2\langle\tau\rangle f}\right)\right\} \tag{C7}$$

Here the excluded probability contribution is similar to (C6) above with K replaced by

$$\kappa = \sum_{m=1}^{\infty}\left[Q\left(R_1, R_2; -\frac{1}{m-\beta}\frac{1}{f\langle\tau\rangle}, -\frac{1}{m+0.5}\frac{1}{f\langle\tau\rangle}\right) + Q\left(R_1, R_2; \frac{1}{m+\beta}\frac{1}{f\langle\tau\rangle}, \frac{1}{m-0.5}\frac{1}{f\langle\tau\rangle}\right)\right] + Q\left(R_1, R_2; -\infty, \frac{-2}{f\langle\tau\rangle}\right) + Q\left(R_1, R_2; \frac{1}{\beta}\frac{1}{f\langle\tau\rangle}, \infty\right) \tag{C8}$$

and $Q(R_1, R_2; T_1, T_2)$ is the integral

$$\int_{R_1}^{R_2} dR \int_{T_1}^{T_2} dT\, p(R, T)$$

as evaluated in Appendix D. The total contribution of these is given by the factor $1 - L$ with

$$L = \int_0^{\infty} dR \int_{T_1}^{T_2} dT\, p(R, T) = \frac{1}{2}\left\{\frac{1-T_1}{[(1-T_1)^2 + T_1{}^2\nu^2]^{1/2}} + \frac{T_2 - 1}{[(T_2-1)^2 + T_2{}^2\nu^2]^{1/2}}\right\} \tag{C9}$$

This number is compared with $1 - K$ in Table 1.

APPENDIX D: INTEGRALS OF $p(R)$, $p(T)$, AND $p(R, T)$

The integral

$$Q(R_1, R_2; T_1, T_2) = \int_{R_1}^{R_2} dR \int_{T_1}^{T_2} dT\, p(R, T) \tag{D1}$$

can be evaluated by substituting

$$u = \frac{1}{\nu}\left(\frac{1}{T} - 1\right) \qquad du = -\frac{dT}{\nu T^2}$$

giving

$$\begin{aligned}\int_{T_1}^{T_2} dT\, p(R, T) &= \int_{(1/T_2-1)/\nu}^{(1/T_1-1)/\nu} du \frac{2}{\sqrt{\pi}} R^2 \exp\left[-R^2(1+u^2)\right] \\ &= Re^{-R^2}\frac{2}{\sqrt{\pi}}\int_{(1/T_2-1)R/\nu}^{(1/T_1-1)R/\nu} dt \exp(-t^2) \\ &= Re^{-R^2}\left\{\operatorname{erf}\left[\frac{R}{\nu}\left(\frac{1}{T_1}-1\right)\right] - \operatorname{erf}\left[\frac{R}{\nu}\left(\frac{1}{T_2}-1\right)\right]\right\}\end{aligned} \tag{D2}$$

Thus (D1) can be integrated by parts, noting that

$$-\frac{1}{2}d(e^{-R^2}) = Re^{-R^2}\,dR$$

$$d[\operatorname{erf}(\alpha R)] = \frac{2}{\sqrt{\pi}}\alpha \exp(-\alpha^2 R^2)\,dR$$

to give the final result

$$\begin{aligned}&\frac{1}{\nu}\left(\frac{1}{T_1}-1\right)\left[1+\frac{1}{\nu^2}\left(\frac{1}{T_1}-1\right)^2\right]^{-0.5} \\ &\quad\cdot\{\operatorname{erf}[R_2(1+(1/T_1-1)^2/\nu^2)^{1/2}] \\ &\quad - \operatorname{erf}[R_1(1+(1/T_1-1)^2/\nu^2)^{1/2}]\} \\ &\quad -\frac{1}{\nu}\left(\frac{1}{T_2}-1\right)\left[1+\frac{1}{\nu^2}\left(\frac{1}{T_2}-1\right)^2\right]^{-0.5} \\ &\quad\cdot\{\operatorname{erf}[R_2(1+(1/T_2-1)^2/\nu^2)^{1/2}] \\ &\quad - \operatorname{erf}[R_1(1+(1/T_2-1)^2/\nu^2)^{1/2}]\} \\ &\quad - e^{-R_2{}^2}\left\{\operatorname{erf}\left[\frac{R_2}{\nu}\left(\frac{1}{T_1}-1\right)\right] - \operatorname{erf}\left[\frac{R_2}{\nu}\left(\frac{1}{T_2}-1\right)\right]\right\} \\ &\quad + e^{-R_1{}^2}\left\{\operatorname{erf}\left[\frac{R_1}{\nu}\left(\frac{1}{T_1}-1\right)\right] - \operatorname{erf}\left[\frac{R_1}{\nu}\left(\frac{1}{T_2}-1\right)\right]\right\} \\ &= 2Q(R_1, R_2; T_1, T_2)\end{aligned} \tag{D3}$$

It can be found in standard integral tables [e.g., *Gradshteyn and Ryzhik*, 1980] that (B3) and (B2) can be integrated to give, respectively,

$$P(T) = \int p(T)\,dT = \tfrac{1}{2}\operatorname{sgn}(T)\frac{T-1}{[(1-T)^2 + \nu^2T^2]^{1/2}} \tag{D4}$$

$$\int p(R)\,dR = -\exp(-R^2) \tag{D5}$$

which is the well-known Rayleigh Distribution.

Acknowledgments. We thank Russ Davis, Lloyd Regier, and George Forristall for making the field data available. This work was supported by National Science Foundation grants OCE-8240404 and MEA-8210649 and by the MIT Sea Grant College Program under grant NA81AA-D-00069 from the Office of Sea Grant, NOAA, Department of Commerce.

REFERENCES

Bingham, C., M. D. Godfrey, and J. W. Tukey, Modern techniques of power spectrum estimation, *IEEE Trans. Audio Electroacoust., AU-15*(2), 56–66, 1967.

Dugundji, J., Envelopes and pre-envelopes of real waveforms, *IRE Trans. Inf. Theory, IT-4*(1), 53–57, 1958.

Forristall, G. Z., On the statistical distribution of wave heights in a storm, *J. Geophys. Res., 83*(C5), 2353–2358, 1978.

Gradshteyn, I. S., and I. M. Ryzhik, *Table of Integrals, Series and Products*, Academic, New York, 1980.

Hamilton, R. C., and E. G. Ward, Ocean gathering program: Quality and reduction of data, Paper presented at the Offshore Technology Conference, Am. Inst. of Min., Metall., and Pet. Eng., Houston, Tex., 1974.

Longuet-Higgins, M. S., On the joint distribution of the periods and amplitudes of sea waves, *J. Geophys. Res., 80*(18), 2688–2694, 1975.

Longuet-Higgins, M. S., On the joint distribution of wave periods and amplitudes in a random wave field, *Proc. R. Soc. London Ser A*, in press, 1983.

Melville, W. K., Wave modulation and breakdown, *J. Fluid Mech., 128*, 489–506, 1983.

Naess, A., On the prediction of extreme responses by the envelope method, paper presented at the Third International Conference on the Behaviour of Offshore Structures, Delft Univ. of Technol., Cambridge, Mass., 1982.

Oppenheim, A. V., and R. W. Schafer, *Digital Signal Processing*, Prentice-Hall, Englewood Cliffs, N. J., 1975.

Patterson, M. M., Oceanographic data from hurricane Camille, paper presented at the Offshore Technology Conference, sponsor, Houston, Tex., 1974.

Shum, K. T., Joint statistics of water waves, Master's thesis, Dep. of Civ. Eng., Mass. Inst. of Technol., Cambridge, 1984.

Tayfun, M. A., Frequency analysis of wave heights based on wave envelope, *J. Geophys. Res., 88*(C12), 7573–7587, 1983.

Ward, E. G., Ocean data gathering program: An overview, paper presented at the Offshore Technology Conference, sponsor, Houston, Tex., 1974.

W. K. Melville and K. T. Shum, Department of Civil Engineering, R. M. Parsons Laboratory, Building 48-15, Massachusetts Institute of Technology, Cambridge, MA 02139.

(Received November 3, 1983;
revised January 19, 1984;
accepted February 8, 1984.)